Title

Honours Literature Review

Thomas D. Schanzer
Supervisor: Prof. Steven Sherwood

School of Physics
Climate Change Research Centre and ARC Centre of Excellence for Climate Extremes
University of New South Wales, Sydney, Australia

Abstract

Text

Contents

1 Introduction and background

1.1 The necessity of parametrisation

The primary task of numerical weather and climate models is to simulate the dynamics of the atmosphere and ocean, which are governed by the Navier-Stokes equations. The algorithm chosen to solve these partial differential equations is known as a model's *dynamical core* (McFarlane 2011). Since analytical solutions to the equations do not exist, the dynamical core necessarily approximates the continuous equations with finite-dimensional, exactly solvable alternatives using one of several possible discretisation schemes (e.g., the finite difference, finite element, finite volume and spectral methods) (Christensen and Zanna 2022). In practice, this usually involves representing the prognostic variables (i.e., those that affect the evolution of the flow) with sets of discrete samples in space and time, whose resolution is constrained by the available computing resources. The unavoidable consequence of discretisation is the loss of information about processes occurring on spatial and temporal scales smaller than the corresponding sampling intervals. These processes are said to be *unresolved*.

It is tempting to naïvely accept the loss of fine-scale information as a necessary sacrifice and hope the dynamical core will still make accurate predictions for the larger, resolved scales. Unfortunately, this too is impossible due to the *nonlinearity* of the governing equations. It is instructive to consider the linear case as a counterexample.

Linear differential equations allow arbitrary superpositions of solutions, meaning that any given solution may be partitioned into high- and low-frequency components, both of which are also solutions. One thus has the freedom to solve for the low-frequency components alone without compromise. This property may be understood more formally using the Fourier transform, defined for a function f of space and time by

$$\tilde{f}(\omega, \boldsymbol{k}) = \int \mathrm{d}t\, \mathrm{d}^3x\, e^{i(\boldsymbol{k}\cdot\boldsymbol{x}-\omega t)} f(t, \boldsymbol{x}),$$

which reduces any linear differential equation to an algebraic equation relating the frequency ω to the wavenumber $\boldsymbol{k}$. Each wavenumber component of the initial state propagates trivially according to its own time dependence $e^{-i(\boldsymbol{k}\cdot\boldsymbol{x}-\omega(\boldsymbol{k})t)}$, *independently of the other components*. The fine-scale dynamics may be safely neglected because they have no influence on the coarse scales.

The consequence of the nonlinearity of the equations governing atmospheric and oceanic flows is, therefore, a coupling of the resolved coarse scales to the unresolved fine scales (McFarlane 2011). This fact may be demonstrated more explicitly by applying so-called *Reynolds averaging* to the equations (Christensen and Zanna 2022). Reynolds averaging decomposes each field q into the sum of a coarse-grained (in space or time) or statistical-ensemble-averaged field $\bar{q}$ and a perturbation q'. Note that $\overline{q'} = 0$ by definition. The coarse-graining operation is assumed to be linear, commute with differentiation and satisfy $\overline{\bar{p}q} = \bar{p}\bar{q}$ for any two fields p and q (Monin and Yaglom 2007). Following the example given by Christensen and Zanna (2022), consider the incompressible Navier-Stokes equations, which have the general form

$$\frac{\partial u_i}{\partial t} + u_j \frac{\partial u_i}{\partial x_j} = \sum f_i,$$
$$\frac{\partial u_i}{\partial x_i} = 0$$

where u_i are the components of the velocity, x_i are the coordinates and f_i are various forces per unit mass. Summation over repeated indices is implied. Applying the decomposition and coarse-graining both

sides of the equations yields

$$\begin{aligned} & \frac{\partial}{\partial x_i}\left(\overline{u_i}+u_i'\right)=0 \\ \Rightarrow \qquad & \frac{\partial \overline{u_i}}{\partial x_i}+\underbrace{\frac{\partial \overline{u_i'}}{\partial x_i}}_{=0}=0 \\ \Rightarrow \qquad & \frac{\partial \overline{u_i}}{\partial x_i}=\frac{\partial u_i'}{\partial x_i}=0 \end{aligned}$$

and

$$\begin{aligned} \sum \overline{f_i} &= \overline{\frac{\partial}{\partial t}\left(\overline{u_i}+u_i'\right)}+\overline{\left(\overline{u_j}+u_j'\right)\frac{\partial}{\partial x_j}\left(\overline{u_i}+u_i'\right)} \\ &= \frac{\partial \overline{u_i}}{\partial t}+\underbrace{\frac{\partial \overline{u_i'}}{\partial t}}_{=0}+\overline{u_j}\frac{\partial \overline{u_i}}{\partial x_j}+\overline{u_j}\underbrace{\frac{\partial \overline{u_i'}}{\partial x_j}}_{=0}+\underbrace{\overline{u_j'}}_{=0}\frac{\partial \overline{u_i}}{\partial x_j}+\overline{u_j'\frac{\partial u_i'}{\partial x_j}} \\ &= \frac{\partial \overline{u_i}}{\partial t}+\overline{u_j}\frac{\partial \overline{u_i}}{\partial x_j}+\frac{\partial \overline{u_i'u_j'}}{\partial x_j}-\overline{u_i'\underbrace{\frac{\partial u_j'}{\partial x_j}}_{=0}} \\ \Leftrightarrow \qquad \frac{\partial \overline{u_i}}{\partial t}+\overline{u_j}\frac{\partial \overline{u_i}}{\partial x_j} &= \sum \overline{f_i}-\frac{\partial \overline{u_i'u_j'}}{\partial x_j}. \end{aligned}$$

The physical meaning of this last equation is that the evolution of the coarse-grained velocity field depends not only on itself and the coarse-grained forces, but also on the perturbations via $\overline{u_i'u_j'}$, which does not necessarily vanish. This dependence is a consequence of nonlinearity.

The theoretical discussion in this section establishes that physical processes occurring at one place in the spectrum of temporal and spatial scales are coupled to all the other processes in the spectrum. In particular, to ignore the effect of processes not explicitly resolved in numerical models would introduce unacceptable systematic biases, or errors, in the model forecasts. Numerical weather and climate models therefore require parametrisation schemes to estimate the effects of unresolved processes as functions of the available large-scale information (and the parameters of these functions must be chosen appropriately—hence the name "parametrisation").

1.2 Physical processes requiring parametrisation

Following the broad theoretical argument in the previous section, I now turn to concrete examples of processes that are often represented by parametrisations, restricting the discussion to atmospheric processes for brevity. This section will give a basic introduction to each process, its effect on the larger-scale behaviour of the climate system and the role of its corresponding parametrisation scheme. The purpose of these examples is to provide real-world context and motivation for current parametrisation research in more idealised settings, which will form one of the main topics of this review.

Cloud microphysics parametrisations model the composition of clouds in terms of the amount of water in the solid (e.g., hail), liquid (cloud droplets and rain) and gaseous phases, and the rate of transitions between these phases. Accurate representation of cloud formation and evolution is crucial for several reasons. First, the interaction of clouds with solar and terrestrial radiation has a major influence on the overall energy balance of the atmosphere (McFarlane 2011). Second, cloud water phase transitions lead to the formation of precipitation, and are a source and sink of latent heat that drives convection (McFarlane 2011). Furthermore, the statistics of cloud formation are linked to global temperatures in a feedback loop; uncertainty in the sign and magnitude of this feedback effect is a major contributor to uncertainty in the sensitivity of global temperatures to increases in atmospheric CO_2 concentration (Andrews et al.

2012; Christensen and Zanna 2022). Microphysical processes occur on the spatial scales of single water droplets and ice particles—among the smallest scales in the atmosphere. All atmospheric models must parametrise the amount of cloud water in each phase, the size distribution and concentration of liquid and ice particles, and the resulting rate and type (rain, hail, snow, etc.) of precipitation (Christensen and Zanna 2022).

Moist convection encompasses vertial motions in the atmosphere that are accompanied (and driven) by phase changes of water, and must be parametrised when it occurs on sub-grid scales. Moist convection is generally triggered by warming and moistening at low levels, which create convective instability, and is manifested by narrow updrafts and downdrafts that can rarely be resolved explicitly (McFarlane 2011). Convection transports heat and moisture vertically, removing the instability and generating storms where the condensed water falls out as precipitation; more broadly, it is a key component of the global atmospheric circulation in spite of its small spatial scale (Christensen and Zanna 2022).

It should be noted that parametrisation also encompasses estimation techniques for processes that are too complex to model exactly for reasons unrelated to spatial and temporal resolution (McFarlane 2011). A good example of such a process is *radiative transfer*. Air and its constituent gases, as well as clouds, absorb, emit, reflect and/or scatter solar and terrestrial radiation. This leads to differential heating and cooling that drives the atmospheric circulation. While the theory of radiative transfer is understood well enough to allow precise calculations in principle, the prohibitive computational cost of such calculations necessitates a parametrisation based on simplifying assumptions (the details of which are beyond the scope of this review) (Christensen and Zanna 2022).

1.3 Traditional solutions to the problem and their limitations

With the examples of cloud microphysics, moist convection and radiative transfer in mind, I now broadly review the traditional approaches used to construct parametrisation schemes in practice. In particular, this section will identify the key assumptions upon which many traditional schemes are founded, and the circumstances under which the assumptions may be violated. This will motivate research into novel approaches.

A parametrisation scheme is traditionally constructed by formulating a simplfied, easily solvable and deterministic conceptual model of the physical process in question. The solution of this model is then used to estimate the effect of the process on the coarse-scale state of the parent model, known as the *unresolved tendency* (McFarlane 2011). For example, the earliest convective parametrisation was developed by Manabe, Smagorinsky, and Strickler (1965) and simply assumed that the net effect of convection is to relax the vertical structure of the atmosphere towards a neutrally stable state whenever it becomes convectively unstable. One obvious deficiency of simple conceptual models is that they cannot possibly capture the full range of variability in the processes they simulate. One major branch of modern parametrisation research therefore studies *data-driven* schemes that instead use observational or high-resolution simulated data to fit empirical models for the unresolved processes, naturally capturing a wider range of variability (Christensen and Zanna 2022). Data-driven parametrisation will be discussed in much further detail in the next section.

In general, a traditional parametrisation scheme aims to capture the net unresolved tendency due to all occurrences of the unresolved process (e.g., all convective updrafts and downdrafts) within each grid cell of the parent model. A deterministic prediction of this type is valid when each grid cell contains many independent realisations whose varying contributions may be expected to yield a reliable average tendency. This requires a *scale separation* between the unresolved process and the resolution of the parent model. Scale separation breaks down when model development and increases in available computing resources allow simulations at resolutions approaching the previously unresolved scales. In this case, knowledge of the coarse-scale state cannot be expected to uniquely determine the unresolved tendency because the process is only realised a few times in each grid cell. The resulting (seemingly) random nature of the true unresolved tendency motivates stochastic treatments (Christensen and Zanna 2022; McFarlane 2011). These will be discussed in the next section.

The conceptual models core to traditional parametrisations usually contain free parameters that are determined from the coarse-scale model state using additional assumptions called *closures*. Closures often postulate a state of quasi-equilibrium between the unresolved processes and their large-scale environment, such as a balance between the accumulation of convective available potential energy (CAPE) and its removal by convection, or between the horizontal convergence of moisture at low levels and its convective transport to higher levels (Christensen and Zanna 2022; McFarlane 2011). However, there is no guarantee that such an equilibrium exists; in fact, it has been demonstrated that the CAPE balance is violated by fluctuations on sub-diurnal time scales (Donner and Phillips 2003) and by midlatitude continental convection (Zhang 2002). Newer parametrisation schemes have allowed departures from equilibrium by representing the unresolved processes in a prognostic rather than diagnostic manner (i.e., allowing the processes to have their own self-governing time dependence rather than calculating them from the large-scale state at each time step independently of their values at the previous step) (Rio, Del Genio, and Hourdin 2019). This creates *memory* or *latency* in the parametrised tendencies, meaning that the tendencies have some nonzero response time when subjected to sudden changes in the large-scale state. Memory will be discussed further in the next section.

Parametrisation schemes commonly suffer from several other issues that I will briefly address here. Firstly, while the division of the general atmospheric dynamics into a set of separately parametrised processes (microphysics, convection, etc.) is physically motivated, it remains somewhat arbitrary because these processes, strictly speaking, form a continuum without well-defined boundaries (Christensen and Zanna 2022; McFarlane 2011). It is a goal of contemporary research to unify the parametrisations as much as possible. Secondly, given the importance of future climate projections, it is natural to ask whether the parametrisation schemes that have been developed and tuned on today's climate remain valid as the climate changes over decade- to century-long simulations. This is a matter of particular concern for data-driven parametrisations, since there is little reason to trust empirical models once they are extrapolated beyond the range of the data originally used to fit them (Christensen and Zanna 2022). Finally, unless very special care is taken, parametrisation schemes can cause the parent model to violate known physical conservation laws (e.g., mass, energy and momentum) (Christensen and Zanna 2022). Efforts to resolve this issue are ongoing.

2 Novel approaches to the parametrisation problem

3 Simple dynamical systems as testbeds for novel approaches

4 Dynamical system case study: Rayleigh-Bénard convection

4.1 Problem statement

Rayleigh-Bénard convection is the motion of a fluid confined between two horizontal isothermal plates, the temperature of the bottom plate being higher than that of the top plate. The governing equations for the flow follow from the Navier-Stokes equations of mass, energy and momentum conservation. The reader is referred to Chandrasekhar (1961) for a detailed derivation; I summarise the assumptions and approximations involved below.

The density, ρ, of the fluid is related to its temperature T by the linear equation of state

$$\rho = \rho_0[1 - \alpha(T - T_0)],$$

where α is the (constant) volume coefficient of thermal expansion and ρ_0 and T_0 are the base-state density and temperature such that $\rho = \rho_0$ when $T = T_0$. The key assumption is that density variations are small ($\alpha(T - T_0) \ll 1$), which allows the governing equations to be simplified under the *Boussinesq approximation*. The Boussinesq approximation involves first writing the pressure, p, of the fluid as

$$p = p_0 - \rho_0 g z + p',$$

where p_0 is an arbitrary constant, g is the acceleration due to gravity and z is the vertical coordinate. p' is the (time-varying) deviation from a hydrostatically balanced background profile $p_0 - \rho_0 g z$ in which the upward pressure gradient force per unit volume $\rho_0 g$ cancels the downward weight force per unit volume $-\rho_0 g$. Since $\alpha(T - T_0) \ll 1$, density variations are neglected everywhere except in their contribution to the weight force, leading to a net buoyant (background pressure gradient plus weight) force per unit mass

$$\frac{\rho_0 - \rho}{\rho_0} g = \alpha(T - T_0) g.$$

With these assumptions in mind, I adopt the governing equations as they are derived by Chandrasekhar (1961):

$$\frac{\partial \boldsymbol{u}}{\partial t} + \boldsymbol{u} \cdot \boldsymbol{\nabla} \boldsymbol{u} = -\frac{1}{\rho_0} \boldsymbol{\nabla} p' + \alpha(T - T_0) g \hat{\boldsymbol{z}} + \nu \nabla^2 \boldsymbol{u} \quad \text{(momentum conservation)}, \tag{4.1}$$

$$\frac{\partial T}{\partial t} + \boldsymbol{u} \cdot \boldsymbol{\nabla} T = \kappa \nabla^2 T \quad \text{(energy conservation), and} \tag{4.2}$$

$$\boldsymbol{\nabla} \cdot \boldsymbol{u} = 0 \quad \text{(incompressibility)}. \tag{4.3}$$

$\boldsymbol{u}$ is the fluid velocity, t is time, $\hat{\boldsymbol{z}}$ is the upward unit vector, ν is the (constant) kinematic viscosity and κ is the thermal diffusivity (also constant). Notice that the aforementioned buoyancy term $\alpha(T - T_0)g$ appears on the right-hand side of (4.1).

The parametrisation test-bed developed in this work solves the governing equations in a two-dimensional domain $(x, z) \in [0, d] \times [0, L]$, subject to no-slip, isothermal boundary conditions on the top and bottom plates,

$$\boldsymbol{u} = \boldsymbol{0}, \quad T = T_0 + \frac{\delta T}{2} \qquad \text{at } z = 0 \text{ and} \tag{4.4}$$

$$\boldsymbol{u} = \boldsymbol{0}, \quad T = T_0 - \frac{\delta T}{2} \qquad \text{at } z = d, \tag{4.5}$$

and periodic boundary conditions in the horizontal,

$$\boldsymbol{u}(x = 0) = \boldsymbol{u}(x = L) \quad \text{and} \quad T(x = 0) = T(x = L). \tag{4.6}$$

δT is the constant temperature difference between the plates.

4.2 Nondimensionalisation and scale analysis

It is helpful to nondimensionalise the governing equations (4.1)–(4.6); this is not only useful for numerical work but also gives insight into the different flow regimes that are possible. A range of nondimensionalisations are used in fluid dynamics literature; I adopt a common one (see, e.g., Grötzbach (1983), Ouertatani et al. (2008), and Stevens, Verzicco, and Lohse (2010)) which is suitable for the turbulent convective regime.

For low-viscosity, turbulent flow, a suitable time scale is the *free-fall time* t_0, which is the time for a fluid element with constant temperature $T = T_0 - \delta T$ to fall from the top plate to the bottom plate under the influence of buoyancy ($-g\alpha\delta T$) alone. It is simple to show that

$$t_0 \sim \left(\frac{d}{g\alpha\delta T}\right)^{1/2},$$

ignoring a factor of $\sqrt{2}$. The obvious length and temperature scales are the plate separation d and temperature difference δT, respectively.

Making the substitutions $p'/\rho_0 \to \pi$ and $T - T_0 \to \theta$ in (4.1)–(4.6) and expressing all variables in units of t_0, d and δT leads to the dimensionless equations

$$\frac{\partial \boldsymbol{u}}{\partial t} + \boldsymbol{u}\cdot\boldsymbol{\nabla}\boldsymbol{u} = -\boldsymbol{\nabla}\pi + \left(\frac{\mathrm{Pr}}{\mathrm{Ra}}\right)^{1/2}\nabla^2\boldsymbol{u} + \theta\hat{\boldsymbol{z}}, \tag{4.7}$$

$$\frac{\partial \theta}{\partial t} + \boldsymbol{u}\cdot\boldsymbol{\nabla}\theta = (\mathrm{Ra}\,\mathrm{Pr})^{-1/2}\nabla^2\theta, \quad \text{and} \tag{4.8}$$

$$\boldsymbol{\nabla}\cdot\boldsymbol{u} = 0, \tag{4.9}$$

with boundary conditions

$$\boldsymbol{u} = \boldsymbol{0}, \quad \theta = +\frac{1}{2} \qquad \text{at } z = 0, \tag{4.10}$$

$$\boldsymbol{u} = \boldsymbol{0}, \quad \theta = -\frac{1}{2} \qquad \text{at } z = 1, \tag{4.11}$$

$$\boldsymbol{u}(x=0) = \boldsymbol{u}(x=\Gamma) \quad \text{and} \quad \theta(x=0) = \theta(x=\Gamma). \tag{4.12}$$

There are three dimensionless parameters: the aspect ratio of the domain

$$\Gamma \equiv \frac{L}{d},$$

the *Prandtl number*

$$\mathrm{Pr} \equiv \frac{\nu}{\kappa}$$

which measures the relative importance of viscosity (momentum diffusivity) and thermal diffusivity, and the *Rayleigh number*

$$\mathrm{Ra} \equiv \frac{g\alpha d^3\delta T}{\kappa\nu}.$$

The Rayleigh number can be interpreted as the ratio of the time scale for thermal transport by convection to the time scale for thermal transport by conduction. It determines the importance of diffusion for the evolution of $\boldsymbol{u}$ and θ; inspection of (4.7) and (4.8) indicates that low Ra implies strong diffusion and high Ra weak diffusion. Detailed theoretical analysis of the governing equations (see, e.g., Chandrasekhar (1961) and the seminal work by Lord Rayleigh (1916)) reveals that there exists a critical Rayleigh number (dependent on boundary conditions but of order 10^3), below which the equations have a stable equilibrium with the fluid at rest and a linear conductive temperature profile. Above the critical value, the equilibrium is unstable and small perturbations lead to the formation of a regular series of steady, rotating convection cells. If the Rayleigh number is increased much further (Le Quéré (1991) cites $\mathrm{Ra} \approx 2 \times 10^8$), the solution becomes unsteady and increasingly turbulent. This work is concerned with the turbulent regime, since Rayleigh numbers for atmospheric deep moist convection can be as large as 10^{22} (Chillà and Schumacher 2012).

4.3 Thermal properties

The rate of heat transport across the fluid layer has physical significance for natural realisations of thermally driven convection. It is widely analysed in terms of the dimensionless *Nusselt number*, whose accurate determination is a common theme in the Rayleigh-Bénard convection literature; I therefore introduce this quantity before proceeding. The Nusselt number measures the rate of (vertical) heat transport across a horizontal plane at height z, normalised by the purely conductive rate that would exist if the fluid were at rest (Verzicco and Camussi 1999). Following Chillà and Schumacher (2012), I use the definition (before nondimensionalisation)

$$\mathrm{Nu}(z,t) \equiv \frac{\langle wT\rangle_{A,t} - \kappa\partial\langle T\rangle_{A,t}/\partial z}{\kappa\delta T/d} \tag{4.13}$$

where $\langle\cdot\rangle_{A,t}$ denotes averaging over time and the horizontal plane at height z, and $w = \boldsymbol{u}\cdot\hat{\boldsymbol{z}}$ is the vertical velocity. The rate of heat transport in the numerator has two terms: advection $\langle wT\rangle_{A,t}$ and conduction $-\kappa\partial\langle T\rangle_{A,t}/\partial z$. The denominator $\kappa\delta T/d$ is the rate of heat transport for a linear conductive temperature profile with the fluid at rest. Scheel, Emran, and Schumacher (2013) give the corresponding nondimensionalised form,

$$\mathrm{Nu}(z,t) \equiv (\mathrm{Ra}\,\mathrm{Pr})^{1/2}\langle w\theta\rangle_{A,t} - \frac{\partial\langle\theta\rangle_{A,t}}{\partial z}. \tag{4.14}$$

Another important quantity is the thickness δ_T of the *thermal boundary layer* at each plate where large temperature gradients exist. Chillà and Schumacher (2012) define δ_T as follows: if, on average, the fluid temperature changes with height from $+\delta T/2$ at the lower plate to 0 (the mean value in the well-mixed interior) over a distance δ_T, then

$$\left.\frac{\partial\langle T\rangle_{A,t}}{\partial z}\right|_{z=0} \approx -\frac{\delta T}{2\delta_T}.$$

But if one considers the definition of the Nusselt number (4.13) at $z = 0$, the advection term $\langle wT\rangle_{A,t}$ vanishes due to the $\boldsymbol{u} = \boldsymbol{0}$ boundary condition and

$$\mathrm{Nu}(z=0) = -\frac{d}{\delta T}\left.\frac{\partial\langle T\rangle_{A,t}}{\partial z}\right|_{z=0}.$$

Thus,

$$\delta_T = \frac{d}{2\,\mathrm{Nu}(z=0)}. \tag{4.15}$$

4.4 Resolution dependence of numerical solutions

In constructing a parametrisation test-bed, I will firstly seek reasonably accurate, high-resolution "truth" solutions of (4.7)–(4.12). I will then deliberately reduce the resolution, aiming to produce solutions that are sufficiently "different" that they might reasonably be "improved" by a parametrisation scheme. In this section, I review relevant literature with the aim of establishing how, exactly, under-resolved simulations of Rayleigh-Bénard convection might "differ" from well-resolved ones, and thus what one would hope to "improve". Specifically, I will address the following questions:

- What resolution is necessary for a converged solution?
- Which quantities are most sensitive to insufficient resolution?

4.4.1 Theoretical resolution requirements for accurate simulations

Grötzbach (1983) is recognised as the first to formulate resolution requirements for accurate simulations of Rayleigh-Bénard convection (Chillà and Schumacher 2012; Scheel, Emran, and Schumacher 2013). He

identified separate constraints on the mean (i.e., averaged in each spatial direction) grid spacing and the vertical spacing near the plates; I first discuss the former. Grötzbach reasoned that a numerical model that neglects subgrid-scale effects must have a geometric mean grid spacing $h = (\Delta x \Delta y \Delta z)^{1/3}$ such that

$$h \leq \pi\eta = \pi \left(\frac{\nu^3}{\langle \epsilon \rangle} \right)^{1/4} \tag{4.16}$$

where $\eta \equiv (\nu^3/\epsilon)^{1/4}$ is the *Kolmogorov length*, the universal smallest relevant length scale for general turbulent flow, and $\langle \epsilon \rangle$ is the spatial and temporal average of the kinetic energy dissipation rate defined by

$$\epsilon(\boldsymbol{x}, t) \equiv \frac{\nu}{2} \sum_{ij} \left(\frac{\partial u_i}{\partial x_j} + \frac{\partial u_j}{\partial x_i} \right)^2 \tag{4.17}$$

(Chillà and Schumacher 2012). The condition (4.16) can be understood using the Nyquist-Shannon theorem, which states that a sampling frequency $f \geq k/\pi$ is needed to unambiguously reconstruct a signal with wavenumber k; substituting $f = 1/h$, $k = 1/\eta$ leads to the claimed relation.

Grötzbach recognised that the above reasoning was only valid for the mean grid spacing; large gradients in temperature and velocity near the top and bottom plates require finer resolution in those regions. The notion of nearness can be formalised using the thermal boundary layer thickness (4.15), and one asks how many grid points are necessary in this layer. Grötzbach did not give a theoretical argument to derive this number but claimed that 3 points are sufficient for turbulent flows. Shishkina et al. (2010) presented a theoretical argument based on the (experimentally and numerically justified) assumption of laminar *Prandtl-Blasius* flow conditions in the boundary layer and were able to calculate the minimum number of grid points (e.g., 9 for $\mathrm{Ra} = 2 \times 10^9$ and $\mathrm{Pr} = 0.7$). The results agreed with criteria derived in previous numerical experiments. Importantly, the results of Shishkina et al. allow *a priori* determination of vertical resolution requirements, potentially bypassing the time-consuming and expensive process of iteratively running simulations, checking their convergence and updating the resolution.

4.4.2 Resolution-dependence tests and consequences of under-resolution

Performing numerical experiments for a 3D fluid layer, Grötzbach found that RMS velocity and Nusselt number were the most sensitive quantities to insufficient mean grid spacing, but even they increased "only slightly" above the values obtained from well-resolved simulations. He concluded that condition (4.16) was overly restrictive and recommended (for $\mathrm{Pr} > 0.59$) the simplified, approximate version

$$h \lesssim 5.23\,\mathrm{Pr}^{-1/4}\mathrm{Ra}^{-0.3205}.$$

Later work also supports the finding that the Nusselt number is sensitive to under-resolution. Even studying only steady-state convective solutions at moderate Rayleigh number, Le Quéré (1991) found that the maximum and minimum Nusselt numbers were most sensitive to changes in resolution and had the largest uncertainty among existing benchmark solutions. Other studies have used the convergence of the Nusselt number as an indicator that the spatial resolution is sufficient to produce an accurate solution (Ouertatani et al. 2008).

Stevens, Verzicco, and Lohse (2010) performed 3D simulations in a finite cylindrical cavity with the aim of reconciling the apparent disagreement between the Nusselt numbers in previous numerical studies and experimental observations. They found that agreement with experiment could be achieved, but only by using a much higher resolution than the previous studies. They offered the physical explanation that horizontally under-resolved simulations produce insufficient thermal diffusion, leading to systematic overestimation of the buoyancy of convective plumes near the side-walls of the cylinder; this results in Nusselt numbers that exceed experimentally observed values. This led them to conclude that the two criteria of Grötzbach (1983)—for mean grid spacing and for the vertical spacing near the upper and lower plates—are not independent; the definition $h = (\Delta x \Delta y \Delta z)^{1/3}$ in (4.16) allows the horizontal spacing to remain relatively coarse near the plates, provided the vertical spacing is small. Since fine horizontal

resolution is also necessary to accurately capture the dynamics of the thin plumes, they proposed that (4.16) be applied with $h = \max(\Delta x, \Delta y, \Delta z)$ instead.

Some more recent work, however, casts doubt on the notion that the Nusselt number is sensitive to under-resolution and that its convergence is a good indicator that the flow is well-resolved. In assessing the performance of several published computational fluid dynamics codes on the Rayleigh-Bénard problem in a cylindrical cavity, Kooij et al. (2018) identified one higher-order code that reproduced the theoretically predicted scaling of Nu as a function of Ra even when the flow was deliberately under-resolved. On the other hand, the presence of numerical artefacts in the instantaneous temperature field near the bottom plate was a clear indicator of insufficient resolution. Figure 1, a reproduction of part of their Figure 5, shows these artefacts.

Scheel, Emran, and Schumacher (2013) performed similar high-resolution simulations for a cylindrical cavity and also found that the Nusselt number, among other global transport properties, were "fairly insensitive to insufficient resolution, as long as the mean Kolmogorov length [was] resolved" (i.e., (4.16) was satisfied). However, they found that the horizontally averaged or local kinetic energy dissipation rate (4.17) and the corresponding thermal dissipation rate

$$\epsilon_T(\boldsymbol{x}, t) \equiv \kappa \sum_i \left(\frac{\partial T}{\partial x_i} \right)^2 \tag{4.18}$$

were much more sensitive, with their convergence requiring even stricter conditions than (4.16).

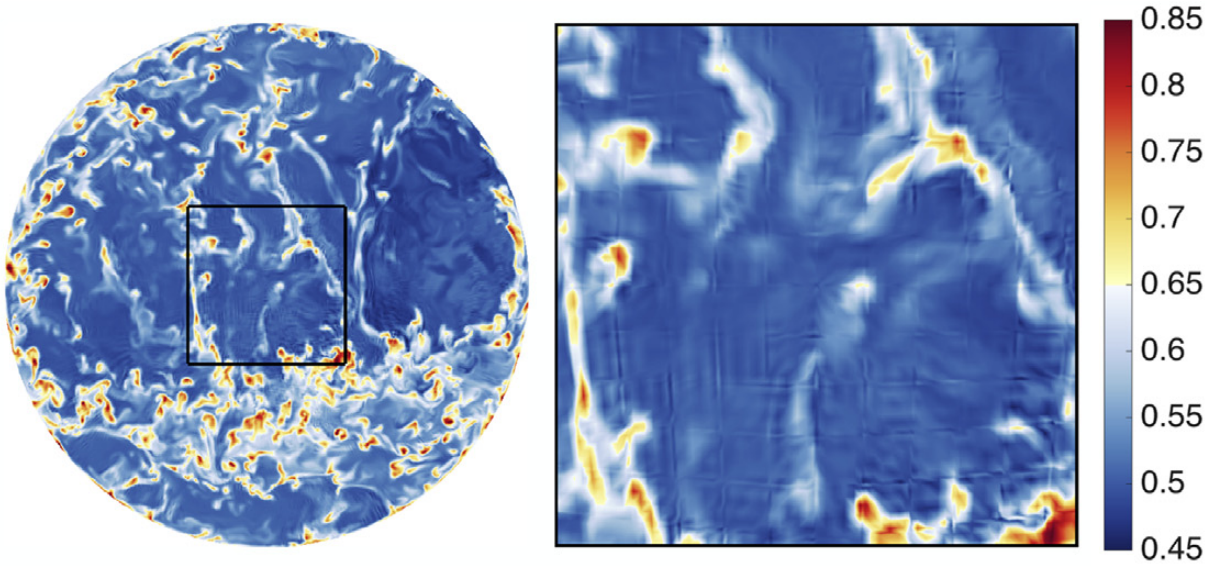

Figure 1: Reproduction of part of Figure 5 by Kooij et al. (2018), showing an instantaneous horizontal temperature profile simulated by the Nek5000 code for Rayleigh-Bénard convection at $\mathrm{Ra} = 10^{10}$. The profile is taken near the bottom plate of a cylindrical cavity and shows a grid-like pattern of numerical artefacts. The right panel is an enlargement of the region inside the black square in the left panel.

5 Conclusion

References

Andrews, T., J. M. Gregory, M. J. Webb, and K. E. Taylor (2012). "Forcing, feedbacks and climate sensitivity in CMIP5 coupled atmosphere-ocean climate models". *Geophys. Res. Lett.* **39**(9). DOI: 10.1029/2012GL051607.

Chandrasekhar, S. (1961). *Hydrodynamic and hydromagnetic stability*. Oxford: Clarendon Press. ISBN: 9780486319209.

Chillà, F. and J. Schumacher (2012). "New perspectives in turbulent Rayleigh-Bénard convection". *Eur. Phys. J. E* **35**(7). DOI: 10.1140/epje/i2012-12058-1.

Christensen, H. and L. Zanna (2022). "Parametrization in weather and climate models". *Oxford Research Encyclopedia of Climate Science*. Oxford University Press. DOI: 10.1093/acrefore/9780190228620.013.826.

Donner, L. J. and V. T. Phillips (2003). "Boundary layer control on convective available potential energy: implications for cumulus parameterization". *J. Geophys. Res.: Atmos.* **108**(D22). DOI: 10.1029/2003JD003773.

Grötzbach, G. (1983). "Spatial resolution requirements for direct numerical simulation of the Rayleigh-Bénard convection". *J. Comput. Phys.* **49**(2). DOI: 10.1016/0021-9991(83)90125-0.

Kooij, G. L., M. A. Botchev, E. M. A. Frederix, B. J. Geurts, S. Horn, D. Lohse, E. P. van der Poel, O. Shishkina, R. J. A. M. Stevens, and R. Verzicco (2018). "Comparison of computational codes for direct numerical simulations of turbulent Rayleigh-Bénard convection". *Comput. Fluids* **166**. DOI: 10.1016/j.compfluid.2018.01.010.

Le Quéré, P. (1991). "Accurate solutions to the square thermally driven cavity at high Rayleigh number". *Comput. Fluids* **20**(1). DOI: 10.1016/0045-7930(91)90025-D.

Lord Rayleigh (1916). "On convection currents in a horizontal layer of fluid, when the higher temperature is on the under side". *Philos. Mag.* **32**(192). DOI: 10.1080/14786441608635602.

Manabe, S., J. Smagorinsky, and R. F. Strickler (1965). "Simulated climatology of a general circulation model with a hydrologic cycle". *Mon. Weather Rev.* **93**(12). DOI: 10.1175/1520-0493(1965)093<0769:SCOAGC>2.3.CO;2.

McFarlane, N. (2011). "Parameterizations: representing key processes in climate models without resolving them". *WIREs Clim. Change* **2**(4). DOI: 10.1002/wcc.122.

Monin, A. S. and A. M. Yaglom (2007). *Statistical fluid mechanics: mechanics of turbulence*. Ed. by J. L. Lumley. Vol. 1. Mineola, New York: Dover Publications. ISBN: 0-486-45883-0.

Ouertatani, N., N. Ben Cheikh, B. Ben Beya, and T. Lili (2008). "Numerical simulation of two-dimensional Rayleigh-Bénard convection in an enclosure". *C.R. Mec.* **336**(5). DOI: 10.1016/j.crme.2008.02.004.

Rio, C., A. D. Del Genio, and F. Hourdin (2019). "Ongoing breakthroughs in convective parameterization". *Curr. Clim. Change Rep.* **5**(2). DOI: 10.1007/s40641-019-00127-w.

Scheel, J. D., M. S. Emran, and J. Schumacher (2013). "Resolving the fine-scale structure in turbulent Rayleigh-Bénard convection". *New J. Phys.* **15**(11). DOI: 10.1088/1367-2630/15/11/113063.

Shishkina, O., R. J. A. M. Stevens, S. Grossmann, and D. Lohse (2010). "Boundary layer structure in turbulent thermal convection and its consequences for the required numerical resolution". *New J. Phys.* **12**(7). DOI: 10.1088/1367-2630/12/7/075022.

Stevens, R. J. A. M., R. Verzicco, and D. Lohse (2010). "Radial boundary layer structure and Nusselt number in Rayleigh-Bénard convection". *J. Fluid Mech.* **643**. DOI: 10.1017/S0022112009992461.

Verzicco, R. and R. Camussi (1999). "Prandtl number effects in convective turbulence". *J. Fluid Mech.* **383**. DOI: 10.1017/S0022112098003619.

Zhang, G. J. (2002). "Convective quasi-equilibrium in midlatitude continental environment and its effect on convective parameterization". *J. Geophys. Res.: Atmos.* **107**(D14). DOI: 10.1029/2001JD001005.